Heliyon 10 (2024) e38214

Contents lists available at ScienceDirect

Heliyon

journal homepage: www.cell.com/heliyon

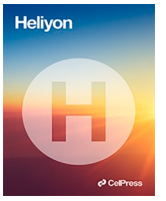

Research article

An open-source combined atomic force microscope and optical microscope for mechanobiology studies

Daniel Delgado [a,1], Sarah Desroches [a,b,1], Gia Kang [a,1], Yousef Aldabii [a], Andrew R. Harris [a,*]

[a] Department of Mechanical and Aerospace Engineering, Carleton University, 1125 Colonel by Drive, Ottawa, Ontario, Canada, K1S 5B6
[b] Ottawa-Carleton Institute for Biomedical Engineering Graduate Program, Carleton University, 1125 Colonel by Drive, Ottawa, Ontario, Canada, K1S 5B6

A B S T R A C T

Atomic Force Microscopy (AFM) has become the gold standard tool for measuring mechanical properties of biological samples including proteins, single cells and tissues. However, investment in this specialized equipment and gaining expertise in its operation are significant obstacles for non-experts looking to adopt this technique. To address this, we have designed an AFM based mechanical measurement system for measuring cell mechanical properties which is combined with a custom inverted fluorescence microscope which can be used for characterizing mechanosensitive responses. This system, through its ease of use and low setup cost, will promote interdisciplinary research leading to new insights into the role of cell mechanics and mechanosensitive responses in physiology and disease.

1. Introduction

Our understanding of the significance of cell mechanical properties and their response to the mechanical environment has been realised through the development of an array of customized experimental tools and techniques. These include, micropipette aspiration [1], magnetic twisting cytometry [2], optical tweezers [3], parallel plate techniques [4] to name but a few [5–7]. These techniques share common features including the ability to precisely measure forces that are relevant to cellular force generation and shape change (pN-nN), operate on the length scale of a cell (10–100 μm), work in physiological conditions (in liquid, at 37 °C), and can often be combined with optical microscopy to observe mechanosensitive cellular responses.

Arguably, the gold standard technique to date used to measure cell mechanical properties is Atomic Force Microscopy (AFM). Because AFM uses a probe that interacts directly with a surface, it lends itself to measuring the properties of adherent cells mounted on glass coverslips and as a result, can easily be combined with inverted optical microscopy techniques [8,9]. AFM has been used to measure mechanical properties of cells such as their elasticity and rheological properties, adhesion forces, and geometrical properties such as cell thickness or volume. For example, AFM has been used to measure the stiffness of benign (MCF-10A) and cancerous (MCF-7) human breast epithelial cells, demonstrating increased stiffness among the benign cells which provides important pathological information [10]. AFM has also been used to measure cell-cell adhesion forces [11], and changes in mechanical properties with the formation of intercellular junctions in epithelial sheets [12]. In other studies, changes in cell thickness and elasticity have been measured using AFM in response to osmotic treatments [13–15]. Together, these measurements have led to important insights into the dependency of cell mechanical properties on the organization of the actin cytoskeleton [16–19], cytosolic pressure [20], and plasma

* Corresponding author.
E-mail address: andrew.harris3@carleton.ca (A.R. Harris).
[1] Equal contribution.

https://doi.org/10.1016/j.heliyon.2024.e38214
Received 30 June 2024; Received in revised form 29 August 2024; Accepted 19 September 2024
Available online 20 September 2024

membrane tension [21].

Unfortunately, the costs and complexity of using mechanical measurement techniques for mechanobiology studies can be a limiting factor preventing their use by non-experts in this field. Various custom low-cost mechanobiology testing and optical microscopy systems have been developed to overcome this barrier, such as the cell stretcher developed by Kah et al. which was mainly built from the parts of an Anet A8 3D printer [22]. Uniaxial stretching with this system demonstrated activation of the YAP mechanotransduction pathway in cells, emphasizing its ability to study complex mechanobiological processes at a reasonable cost. The Flexiscope is a microscopy system developed by Courtney et al. which can be reconfigured depending on the requirements associated with the experimental design, while producing high-quality fluorescent images in combination with micromaniuplation [23]. Additional low-cost optical systems have also been developed including 3D printed incubator microscopes [24], a spinning disk confocal microscope [25] and a structured illumination microscope [26]. In terms of AFM, several low cost systems have been developed both for conceptual demonstration [27], educational purposes [28] and materials science research [29]. However, these examples of low-cost AFM systems are not well suited for mechanobiology studies as they are either not combined with optical microscopy or lack the ability to operate in liquid.

To address these challenges, we have built a customized combined AFM and inverted fluorescence microscope for mechanobiology studies. The goal of this system is to enable cell and tissue mechanical measurements for non-experts at relatively low cost, and with open access to software and hardware for customizable control and experiments. We provide a full description of this system and examples of experimental measurements that can be made.

2. Results

The device consists of two major components: the atomic force microscope system for measuring the mechanical properties of the cells and mechanical stimulation, and the optical microscope system for imaging the response of the sample.

2.1. Atomic force microscope system

We built an AFM that can be used for measuring cell mechanical properties using force distance measurements. The AFM consists of a laser module (laser source and focussing optics), detector module (focussing optics and 4 quadrant photodiode), and a three-axis translational stage which has both manual coarse control and fine electronic control. The laser module was based on a previously developed educational AFM (edu-AFM) available from ThorLabs and was redesigned to be compatible with optically transparent samples and an inverted microscope. A 635 nm 2.5 mW class 3R laser source coupled to an optical fiber was passed through a 0.15NA 633 nm collimator and mounted onto a 6-axis stage. To facilitate simple alignment of the laser onto the back of the cantilever, the stage mount was centered vertically above the center of the cantilever holder. This enables the laser spot to be imaged with the inverted microscope, described in the 'Optical System' section, and precisely aligned onto the cantilever. The reflected laser light from the cantilever was steered with an adjustable mirror into the collecting optics of the detector module. The laser module and detector module were mounted onto a base plate that was either machined from aluminum or 3D printed in Polylactic acid (PLA). The base plate was in turn mounted onto a 3-axis (nanomax) stage, allowing for positioning of the AFM relative to the sample both manually (with coarse and fine control) and electronically (using the piezoelectric stages of the nanomax). This entire assembly was mounted

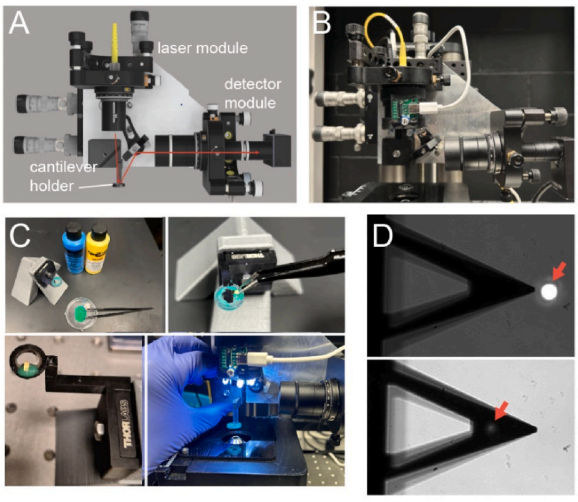

Fig. 1. AFM System. (A) A schematic of the AFM module and its component; the laser light path is indicated in red. (B) A side view photograph of the AFM setup. (C) The cantilever holder (left) and a photograph of the cantilever placement on the holder (right). The cantilever chip was affixed to the holder using reprorubber thin pour biocompatible glue and then mounted with magnets onto the AFM system. (D) The laser dot could be easily visualized and focussed with the optical system onto the back of the cantilever.

onto a high load z-stage which enables the system to be coarsely raised and lowered when changing the sample or the cantilever. The assembled AFM system schematic is shown in Fig. 1A and a photo of the system in Fig. 1B.

The cantilever holder was designed and printed in resin using stereolithography 3D printing which enables sufficient resolution for creating flat surfaces to attach the cantilever. The mounting surface of the cantilever was tilted at an angle of ~12° allowing the reflected laser light to be steered towards the mirror and collection optics. Cantilevers were affixed to the holder using a biocompatible glue (reprorubber thin pour, Fig. 1C). A coverslip was used above the mounting surface of the cantilever to provide a transparent surface enabling the laser to be aligned and imaged with the inverted microscope (Fig. 1D). A key advantage of this setup is that it enables transmitted light imaging, immersion of the cantilever in liquid, and simple alignment of the laser optics.

To calibrate the AFM system, we performed force-distance measurements on glass substrates in order to convert deflection voltages measured on the photodiode to force ('Methods', Fig. 2 A). Our system showed low levels of noise (~200 pN) for the chosen cantilever which is an acceptable range for force-distance measurements on cells that use an indentation setpoint force of 0.5–5 nN (Fig. 2B). To validate our system, we chose to measure the Young's modulus of not only cells but other biomaterials and compared our values to those obtained with a commercial testing system and those reported in the scientific literature. We measured the Young's modulus of polydimethylsiloxane (PDMS) elastomers using the AFM by performing force-distance measurements (Fig. 2C). We compared the results to values obtained from a CellScale UniVert bulk mechanical testing system as a comparison (see 'Methods' under 'Preparing PDMS Substrates', 'AFM Force Curve Measurements and Analyis', 'UniVert Measurements'). The Young's modulus values obtained using the two mechanical testing systems were similar, albeit with a small but significant increase in the value obtained using the AFM system, perhaps due to differences in making local indentation measurements versus bulk compression (AFM: 1094 ± 158 kPa; CellScale: 940 ± 61 kPa; Fig. 2D). Both values however were consistent with previous measurements for PDMS mixing ratio that was used [30]. These results provide confidence that our custom-built system is working correctly and can be used for measuring the mechanical properties of cells and biomaterials.

2.2. Optical system

We built an inverted optical microscope (Fig. 3A) to image and measure cellular response to mechanical stimulation. The optical system allows the AFM user to image cell interactions with the cantilever tip during indentation measurements and facilitates initial calibration of the AFM for alignment and positioning of the laser spot onto the back of the cantilever. This optical system can function with both transmitted light and fluorescence (Fig. 3B), facilitating a variety of different experiments with various cell lines. The initial design of the inverted optical microscope was based on the Flexiscope developed by Courtney et al. adapted to an inverted configuration in order to be compatible with the AFM system [23]. For our setup, the optical system was equipped with a ThorLabs CS165MU/M − Zelux 1.6 MP Monochrome CMOS camera and a Nikon PlanFluor 20x objective and a 470 nm LED for fluorescence illumination. At this magnification, we calculated the system's pixel size to be 0.146 μm using a United States Air Force (USAF) 1951 target (Fig. 3C) following the protocol outlined in 'Methods' under 'Optical System Resolution Calculation'. The sensitivity of the system was measured using green fluorescent protein (GFP) by performing a series of serial dilutions (see 'Methods' under 'Optical System Sensitivity'). For an exposure time of 500 ms, a concentration of 0 μM GFP produced a pixel intensity value of approximately 200. At a GFP concentration of 12.5 μM, the pixel intensity value was saturated at 1022 (Fig. 3D, green line). A Nyquist Sampling

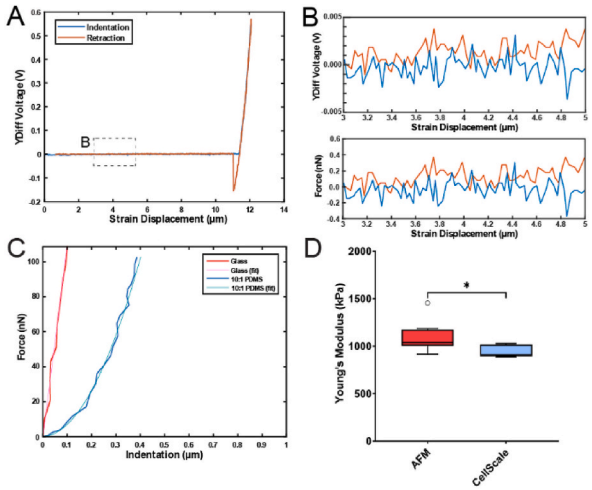

Fig. 2. Force-distance Measurements. (A) Indentation (blue) and retraction (orange) voltages measured on the 4-quadrant-photodiode vs displacement curves recorded from AFM measurements on a glass surface. (B) Zoom in view of the non-contact portion of the curves showing the level of deflection noise in system. (C) The contact region portions of the force vs indentation curves obtained from measurements on glass and 10:1 PDMS (Sylgard 184) surfaces. (D) The Young's modulus of 10:1 PDMS measured with pyramidal tip cantilever (labeled AFM on figure) and with CellScale UniVert system (labeled CellScale). Statistical significance is indicated by asterisk ($p = 0.021$).

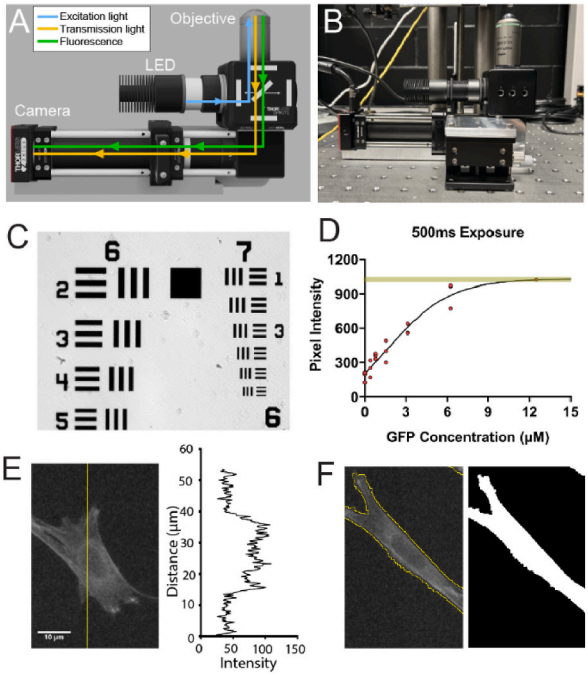

Fig. 3. Optical system. (A) A schematic demonstrating the LED excitation light path, transmission light path, and fluorescence light path for the inverted fluorescence microscope configuration. (B) An image of the inverted fluorescence microscope configuration that sits beneath the sample stage and AFM. (C) An example image of the USAF 1951 Target used to determine the pixel size imaged with the optical system. (D) The maximum pixel intensity detected for a series of GFP serial dilutions in PBS at an exposure of 500 ms, with a sigmoidal line fitted to the data (black line). The saturation value for the camera is shown by the green horizontal line. (E) An image of a Lifeact-GFP expressing cell next to a linescan showing the intensity values. (F) Identification of the cell boundary using intensity thresholding.

Theorem calculation was performed to determine the magnification required to accurately reconstruct signal from the optical system. To satisfy the Nyquist-2 criterion, a magnification of 11.09× is required. To satisfy the Nyquist-3 criterion, a magnification of 16.63× is required. The Nikon Plan Fluor 20x/0.50 objective on the optical system therefore satisfies both Nyquist-2 and Nyquist-3 sampling criteria. The sensitivity of the imaging system provided a suitable signal to noise ratio for imaging single cells expressing Lifeact-GFP (Fig. 3E) and for segmenting cell boundaries using intensity thresholding (Fig. 3F). Taken together, these data show that the optical system was both sensitive and had sufficient resolution for imaging single cells.

2.3. *Measuring changes in cell thickness and elasticity with pharmacological treatments*

We next decided to use the AFM system to make measurements of mechanical properties on 3T3 fibroblasts expressing Lifeact fused to Green Fluorescent Protein (GFP) which is a commonly used marker for actin in live cells (Fig. 4A). Lifeact GFP imaged with our system showed similar subcellular structures as cells fixed and labeled with phalloidin (Fig. 4B). We performed cytoskeletal drug treatments on LifeAct-3T3 GFP cells (Fig. 4C and D) and measured cell thickness and Young's modulus (see 'Methods' under 'Cell Thickness Measurements'). Treatment with both the ROCK inhibitor Y-27632 which inhibits contractility, and depolymerization of actin filaments with Latrunculin B caused a significant change in cell thickness compared to the control (Control: 9.19 ± 2.40 μm; Y-27632: 7.38 ± 1.47 μm, $p < 0.0001$; Latrunculin B: 15.44 ± 2.84 μm, $p < 0.0001$; Fig. 4D). A similar experiment was performed using LifeAct-3T3 GFP cells that underwent hypertonic and hypotonic treatments, and a significant change in cell thickness was also observed for these conditions (Hypo-osmotic: 14.34 ± 2.07 μm, $p < 0.0001$; Hyperosmotic (round): 13.35 ± 2.41 μm, $p < 0.0001$; Hyperosmotic (flat): 7.38 ± 1.76 μm, $p < 0.0001$; Fig. 4E). Cell Young's modulus was then measured for cells that had undergone either cytoskeletal drug treatments or osmotic treatments ('Methods' under 'AFM Force Curve Measurements and Analysis'). Cells that had undergone a Latrunculin B treatment were measured to have a significantly lower Young's modulus compared to the control (Control: 1663.7 ± 1174.7 Pa; Latrunculin B: 645.6 ± 334.02 Pa, $p < 0.0001$; Fig. 4F). A significant change in Young's modulus was also observed on cells that had undergone hypo-osmotic and hyperosmotic treatments (Fig. 4G). The absolute measurements of Young's modulus for these 3T3 cells are within the range of values reported in the literature [31], and our system could be used to measure changes in cell thickness and mechanical properties under different conditions. In addition to observing changes in cell mechanical properties using AFM mechanical measurements, our imaging system offered sufficient resolution and sensitivity to measure changes in cytoskeletal organization following both drug treatments and in different osmotic conditions (Fig. 5).

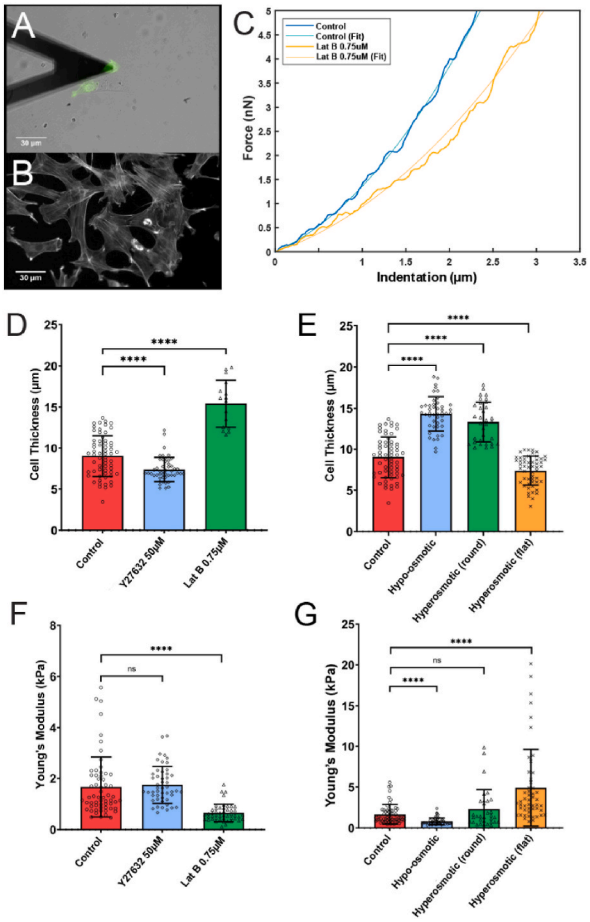

Fig. 4. AFM measurements on cells. (A) Example image of cantilever placement during a mechanical measurement on a 3T3 LifeAct GFP cell. A brightfield image was taken at an exposure of 150 ms and is overlayed with a fluorescent image taken at 500 ms (shown in green). (B) Example image of 3T3 cells stained with phalloidin 488 taken at an exposure of 500 ms. (C) Force vs indentation curve obtained from a measurement on an untreated 3T3 LifeAct GFP cell (blue) and on 3T3 LifeAct GFP cell treated with 0.75 µM Latrunculin B (yellow). Cell thickness measurements in 3T3 LifeAct GFP cells for cytoskeletal drugs (D) and osmotic treatments (E). Cell Young's modulus measurements on LifeAct 3T3 GFP cells treated with cytoskeletal drugs (F) or different osmotic treatments (G). In D-G, statistical significance is indicated as follows; ****: $p < 0.0001$; na: not statistically significant.

3. Discussion

Despite the benefits of AFM based mechanical measurements, its use is often limited to labs specialized in this area and there are several reasons for this. Firstly, the high capital cost of obtaining an AFM system poses a significant barrier to its use by labs which do not have prior expertise in operating the system. We have designed an AFM system that can be built at relatively low cost with off the shelf and 3D printed components. At the time of writing the combined AFM and optical microscope system including the optical breadboard and several fluorescence filter sets cost ~$18k USD, which is an order of magnitude less than a commercially available AFM system alone. Secondly, using AFM in combination with an inverted fluorescence microscope often requires a custom stage to be used on the microscope, making this a dedicated system and difficult to switch between other microscopy experiments and AFM based cell mechanical measurements. We incorporated a dedicated optical microscope into our system that both improves ease of use for alignment and allows for the user to characterize the biological response of the sample. This system could operate both in fluorescence and transmitted light and simplified the alignment procedure for the AFM system. Thirdly, cell mechanical measurements including AFM can be inherently challenging and require step by step procedures and the correct analysis and interpretation of force distance curves [32–34]. We include a detailed description of our experimental methods using this system, the operating software and a list of parts on our Github. Altogether, this system, through its simple operation but high sensitivity and low setup cost can be easily adopted by labs looking to make cell and tissue mechanical measurements. Furthermore, open access and modular nature of the system will enable further modification and customization by expert users, broadening the scope of experimental measurements that can be made with this system.

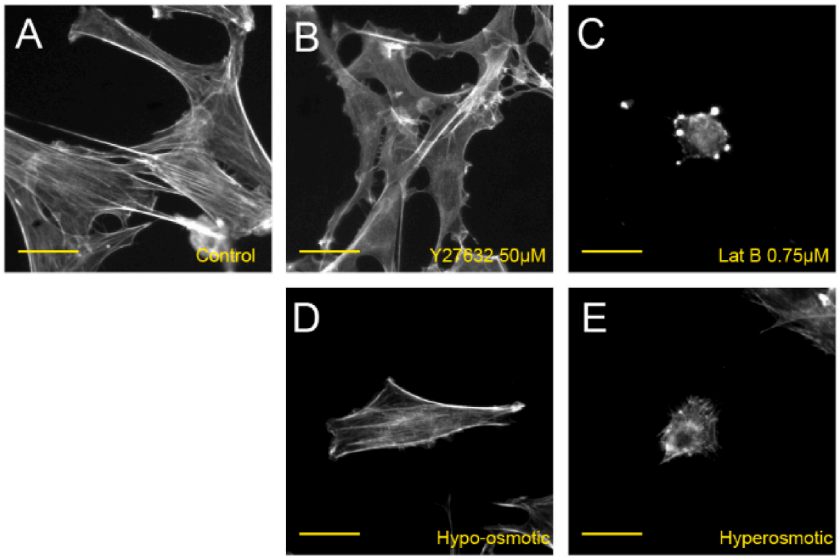

Fig. 5. Microscopy images of cells in different conditions. Optical microscopy images of NIH-3T3 wild type fibroblasts fixed and stained with Phalloidin-AlexaFluor488 showing (A) untreated, (B) treated with 50 μM Y27632, (C) treated with 0.75 μM Latrunculin B, (D, E) different osmotic treatments. Scale bars are 20 μm.

4. Methods

4.1. AFM force curve measurements and analysis

To determine the cell Young's modulus of the sample from force-distance curves, the post-contact region of the force-distance curve was fitted with the Bilodeau model for pyramidal contact to determine the Young's modulus, E, using the following equation [32,35]:

$$F_{pyramidal} = \frac{1.4906\ E\ tan\,(\Phi)}{2(1-\nu^2)}\,\delta^2$$

Where F is force, δ is indentation depth, ν is Poisson's ratio, and $\mathbf{\Phi}$ is the opening angle of the pyramidal tip. To ensure the analysis is performed on the pertinent section of the non-linear region, the fitting was limited to segment of the curve where $F < 5\times 10^{-9}$ N.

The contact point was determined using a MATLAB script based on the algorithm developed by Lin et al. (2006), using least squares minimisation [32]. For every point in the curve, a linear regression model and a Hertz model was fitted to the left and to the right of the point of interest respectively. The sum of the error of the two fits was calculated for every point, and the point with the least summed error was chosen as the contact point. The section of the curve to the right of the contact point was subsequently taken to be the post-contact region.

4.2. Cell thickness measurements

For each cell measurement, a corresponding measurement was collected on the glass surface in a region in close proximity to the cell perimeter. These measurements were made using just the z-piezo without moving the manual z control between measurements. Given that the cell and glass measurements have the same starting point of piezo-displacement $z = 0$, the cell thickness h may be calculated as the difference between the z values of the contact points (z_{cp}) from the respective curves.

$$Cell\ thickness = z_{cp\ cell} - z_{cp\ glass}$$

4.3. Cell culture

NIH-3T3 wild type fibroblast cells and NIH-3T3 LifeAct GFP cells were cultured in DMEM supplemented with 10 % Fetal Bovine Serum (FBS) and 1 % penicillin-streptomycin (PS) solution, at 37 °C in 5 % CO_2, and passaged when confluent using 0.25 % Trypsin-EDTA solution. For AFM testing on glass-bottom 55 mm petri dishes, cells were plated at a density of ~1 x 10^5 cells per dish 24 h prior to performing tests. When ready to perform the AFM testing, the DMEM in each dish was removed and replaced with 3 mL of Leibovitz (GIBCO, #21083027) media supplemented with 10 % FBS. For fluorescent imaging with the AFM system, cells were plated in a glass-bottom 8-well chamber at a density of 3 x 10^4 per well in DMEM supplemented with FBS and PS. The cells were subsequently fixed and stained (Fig. 4B) following the 'Immunostaining' protocol described below.

4.4. Immunostaining

NIH-3T3 fibroblast cells were fixed in 4 % PFA in cell culture water supplemented with 10 % cytoskeleton buffer (10 mM PIPES/KOH, 100 mM NaCl, 300 mM sucrose, 1 mM EGTA, and 1 mM $MgCl_2$ in distilled H_2O) and 0.1 mg/mL sucrose for 20 min at 4 °C. Cells were then washed 3 times with PBS, and permeabilized with 0.1 % Triton X-100 in PBS for 20 min at 4 °C. Cells were again washed 3 times with PBS and subsequently blocked with 2 mg/mL BSA in PBS for 1 h at 4 °C. Cells were then stained with Phalloidin-AlexaFluor 488 (Abcam, ab176753) at a 1:100 dilution in 2 mg/mL BSA in PBS for 1 h at 4 °C. Prior to imaging, the staining solution was removed from each well and rinsed twice with PBS and subsequently replaced with PBS.

4.5. Cytoskeletal drug treatments

To test the role of different cytoskeletal structures on cell mechanical properties, pharmacological treatments were used. At least 30 min prior to performing the AFM tests, the cytoskeletal drugs were added to the Leibovitz media at the following concentrations: 0.75 μM Latrunculin B (Abcam, ab144291) and 50 μM Y-27632 ROCK inhibitor (Abcam, ab120129). The AFM tests were then performed with the Leibovitz solution with the working concentration of cytoskeletal drug. To obtain microscopy images of cells that had undergone cytoskeletal drug treatments, the cells were incubated with the working concentration of cytoskeletal drug in DMEM for 30 min. The cells were then prepared for imaging according to the protocol described in 'Methods' under 'Immunostaining'.

4.6. Osmotic treatments

AFM testing was also performed on cells that had undergone osmotic treatments to test their impact on cellular mechanical properties. At least 30 min prior to performing the AFM tests, the cell culture media in each dish was replaced with either a 1:1 ratio of cell culture water and Leibovitz (hypo-osmotic) or a 0.5M solution of sucrose (Ward's science 57-50-1) in Leibovitz (hyperosmotic). The AFM tests were then performed with the Leibovitz and osmotic treatment solution. To obtain microscopy images of cells that had undergone osmotic treatments, the cells were incubated with DMEM and either cell culture water or 0.5M sucrose for 30 min. The cells were then prepared for imaging according to the protocol described in 'Methods' under 'Immunostaining'.

4.7. Preparing PDMS substrates

Polydimethylsiloxane (PDMS) substrates were prepared using Sylgard 184 (Dow Corning). The desired base to curing agent ratio of 10:1 was weighed separately and then mixed in a conical bottom tube. The PDMS solution was spun in a centrifuge at 300 g for 3 min to remove any air bubbles. The solution was then poured into a 55 mm plastic bottom Petri dish until approximately half of the dish was filled (4–6 mm). The samples were immediately cured by baking at 60 °C for 2–3 h and then sitting at room temperature for an additional 24 h. Once cured, cylindrical PDMS samples were cut and removed by using a 13.5 mm circular biopsy punch.

4.8. PDMS acetone treatment

PDMS samples underwent an acetone treatment which removes excess curing agent to minimize adhesion to the cantilever during AFM testing. Once cylindrical PDMS samples were cut, they were soaked for approximately 16 h in 100 % acetone. The samples were then baked at 60 °C for 3 h prior to UniVert and AFM testing. The PDMS acetone treatment protocol was adapted from Makhija et al. (2018) [36].

4.9. UniVert experiments

The cylindrical PDMS samples were tested on a CellScale UniVert mechanical testing system to determine the stiffness of each sample. Two delicate task wipe pieces were cut to the size of each sample and placed between the compression platens and PDMS to limit adhesion during testing. Quasi-static compressive testing was then performed on each sample to a magnitude of 20 % strain. The duration was set to 50 s, with a relaxation time of 10 s following compression.

Following data collection, a stress-strain plot was generated for each PDMS sample and test repetition. The Young's modulus was determined by calculating the slope of a line fitted to the linear region of the stress-strain curve for each test.

4.10. Statistical analysis

Data are presented as mean ± standard deviation. Unpaired two-tailed t-tests with Welch's correction were performed to assess statistical significance between samples, and p-values of <0.05 were considered significant.

4.11. Imaging experiments

AFM imaging experiments were performed using a Nikon Plan Fluor 20x/0.50 OFN25 DIC N2 objective, a ThorLabs CS165MU/M – Zelux 1.6 MP Monochrome CMOS camera, and the Micro-Manager imaging software. For transmitted light imaging, an in-house built illumination system was used to illuminate the sample. For fluorescent imaging of samples expressing Phalloidin-488 or GFP,

a ThorLabs M470L5 LED was used to illuminate the sample along with a Chroma 39000 series AlexaFluor 488 bandpass filter.

4.12. Nyquist sampling criterion calculation

The minimum resolvable distance, *d*, can be calculated using the following equation:

$$d = \frac{0.61\ \lambda_{emission}}{NA}$$

Where *NA* indicates the numerical aperture of the objective and $\lambda_{emission}$ indicates the emission wavelength of the fluorophore. The minimum resolvable distance was calculated to be 0.62 μm based on the GFP emission wavelength of 510 nm using a 0.5NA objective.

A Nyquist Sampling Theorem calculation was performed to determine the magnification required to accurately reconstruct signal with the ThorLabs CS165MU/M – Zelux 1.6 MP Monochrome CMOS camera. The required magnification to satisfy the Nyquist-2 and Nyquist-3 sampling criteria was determined. To determine the required magnification to satisfy Nyquist-2, the following equation was used:

$$M = 2 \times \frac{P}{d}$$

Where *M* indicates magnification, *d* indicates minimum resolvable distance for the optical system, and *P* indicates the pixel size of the detector being used. The magnification required to satisfy Nyquist-3 can be calculated with the same equation, using a value of 3 instead of 2.

4.13. Optical system resolution calculation

A USAF 1951 target was used to determine the resolution of the optical system (Fig. 3C), by measuring the distance in pixels between line-pairs in various groups and elements using Micro-Manager. ThorLabs provides a line-pair/mm value for each element and group number on the USAF target. The distance between line-pairs in pixels and the line-pair/mm value can then be used to determine pixel size in μm.

$$Resolution\left(\frac{px}{mm}\right) = \frac{Pixels}{Line\ pair} * \frac{Line\ pair}{mm}$$

Where, the line pair per millimeter value is obtained through the manufacture and varies depending on the group and element number being observed by the microscope. Furthermore, the pixels per line pair is determined through the observation and measurement tool of micromanager to determine the pixel distance for one line pair to the above associated element and group. This yields a resolution in px/mm which can be divided out to find the measurement value of one pixel of which with a 20x magnification objective with 0.50NA yielded a 0.166μm/px value.

4.14. Optical system sensitivity

The system's sensitivity to GFP was measured through a series of serial dilutions (Fig. 3D). GFP was diluted in phosphate buffered saline (PBS) to various concentrations ranging from 25 μM to 0 μM. The maximum pixel intensity value in Micro-Manager was recorded for each concentration at an exposure of 500 ms. GFP protein was a kind gift from Adam Stevens (UCSF).

Data availability statement

The datasets generated during and/or analysed during the current study are available from the corresponding author on reasonable request. The schematics for the design, 3D drawings and code are available online through GitHub.

CRediT authorship contribution statement

Daniel Delgado: Writing – original draft, Validation, Methodology. **Sarah Desroches:** Writing – original draft, Validation, Methodology. **Gia Kang:** Writing – original draft, Validation, Methodology. **Yousef Aldabii:** Methodology. **Andrew R. Harris:** Writing – original draft, Supervision, Methodology, Funding acquisition, Conceptualization.

Declaration of competing interest

The authors declare that they have no known competing financial interests or personal relationships that could have appeared to influence the work reported in this paper.

Acknowledgements

A.R.H. gratefully acknowledges support from NSERC (RGPIN-2022-04933). This work was supported by the Banting Foundation Discovery award program. D.D. was supported an NSERC Undergraduate Student Research Award, Y.A. and D.D were supported by the I-CUREUS program at Carleton University. S.D. was supported by an Ontario Graduate Scholarship. The authors would like to thank Eng Kuan Moo for his feedback on the manuscript.

References

[1] R.M. Hochmuth, Micropipette aspiration of living cells, J. Biomech. 33 (2000) 15–22.
[2] X. Trepat, et al., Universal physical responses to stretch in the living cell, Nature 447 (2007) 592–595.
[3] H. Zhang, K.-K. Liu, Optical tweezers for single cells, J. R. Soc. Interface 5 (2008) 671–690.
[4] N. Bufi, P. Durand-Smet, A. Asnacios, Single-cell mechanics: the parallel plates technique, in: Methods in Cell Biology, vol. 125, Elsevier, 2015, pp. 187–209.
[5] E. Moeendarbary, A.R. Harris, Cell mechanics: principles, practices, and prospects, Wiley Interdisciplinary Reviews: Systems Biology and Medicine 6 (2014) 371–388.
[6] T.P. Lele, et al., Tools to study cell mechanics and mechanotransduction, Methods Cell Biol. 83 (2007) 441–472.
[7] P.-H. Wu, et al., Comparative study of cell mechanics methods, Nat. Methods 15 (2018) 491.
[8] N. Gavara, R.S. Chadwick, Determination of the elastic moduli of thin samples and adherent cells using conical atomic force microscope tips, Nat. Nanotechnol. 7 (2012) 733–736.
[9] Y. Suzuki, et al., High-speed atomic force microscopy combined with inverted optical microscopy for studying cellular events, Sci. Rep. 3 (2013) 2131.
[10] Q.S. Li, G.Y. Lee, C.N. Ong, C.T. Lim, AFM indentation study of breast cancer cells, Biochem. Biophys. Res. Commun. 374 (2008) 609–613.
[11] P.-H. Puech, K. Poole, D. Knebel, D.J. Muller, A new technical approach to quantify cell–cell adhesion forces by AFM, Ultramicroscopy 106 (2006) 637–644.
[12] A.R. Harris, A. Daeden, G.T. Charras, Formation of adherens junctions leads to the emergence of a tissue-level tension in epithelial monolayers, J. Cell Sci. 127 (2014) 2507–2517.
[13] T.D. Nguyen, A. Oloyede, S. Singh, Y. Gu, Investigation of the effects of extracellular osmotic pressure on morphology and mechanical properties of individual chondrocyte, Cell Biochem. Biophys. 74 (2016) 229–240.
[14] M.H. Esteki, et al., Poroelastic osmoregulation of living cell volume, iScience 24 (2021).
[15] E. Moeendarbary, et al., The cytoplasm of living cells behaves as a poroelastic material, Nat. Mater. 12 (2013) 253–261.
[16] A.R. Harris, P. Jreij, D.A. Fletcher, Mechanotransduction by the actin cytoskeleton: converting mechanical stimuli into biochemical signals, Annu. Rev. Biophys. 47 (2018) 617–631.
[17] S. Desroches, A.R. Harris, Quantifying cytoskeletal organization from optical microscopy data, Front. Cell Dev. Biol. 11 (2024) 1327994.
[18] D.A. Fletcher, R.D. Mullins, Cell mechanics and the cytoskeleton, Nature 463 (2010) 485–492.
[19] M. Kelkar, P. Bohec, G. Charras, Mechanics of the cellular actin cortex: from signalling to shape change, Curr. Opin. Cell Biol. 66 (2020) 69–78.
[20] G.T. Charras, J.C. Yarrow, M.A. Horton, L. Mahadevan, T.J. Mitchison, Non-equilibration of hydrostatic pressure in blebbing cells, Nature 435 (2005) 365–369.
[21] A. Diz-Muñoz, et al., Membrane tension acts through PLD2 and mTORC2 to limit actin network assembly during neutrophil migration, PLoS Biol. 14 (2016) e1002474.
[22] D. Kah, et al., A low-cost uniaxial cell stretcher for six parallel wells, HardwareX 9 (2021) e00162.
[23] A. Courtney, L.M. Alvey, G.O. Merces, N. Burke, M. Pickering, The Flexiscope: a low cost, flexible, convertible and modular microscope with automated scanning and micromanipulation, R. Soc. Open Sci. 7 (2020) 191949.
[24] B. Diederich, et al., A versatile and customizable low-cost 3D-printed open standard for microscopic imaging, Nat. Commun. 11 (2020) 5979.
[25] A.R. Halpern, et al., Versatile, do-it-yourself, low-cost spinning disk confocal microscope, Biomed. Opt Express 13 (2022) 1102–1120.
[26] S. Hu, et al., Compact and low-cost structured illumination microscopy using an optical fiber coupler, Opt Commun. 436 (2019) 227–231.
[27] T.-H. Hsieh, Y.-C. Tsai, C.-J. Kao, Y.-M. Chang, Y.-W. Lu, A conceptual atomic force microscope using LEGO for nanoscience education, Int. J. Autom. Smart Technol 4 (2014) 113–121.
[28] F. Xia, et al., A modular low-cost atomic force microscope for precision mechatronics education, Mechatronics 76 (2021) 102550.
[29] H.-S. Liao, et al., Open-source controller for low-cost and high-speed atomic force microscopy imaging of skin corneocyte nanotextures, HardwareX 12 (2022) e00341.
[30] F.C. Sales, R.M. Ariati, V.T. Noronha, J.E. Ribeiro, Mechanical characterization of PDMS with different mixing ratios, Procedia Struct. Integr. 37 (2022) 383–388.
[31] A.J. Ford, P. Rajagopalan, Measuring cytoplasmic stiffness of fibroblasts as a function of location and substrate rigidity using atomic force microscopy, ACS Biomater. Sci. Eng. 4 (2018) 3974–3982.
[32] D.C. Lin, E.K. Dimitriadis, F. Horkay, Robust strategies for automated AFM force curve analysis—I. Non-adhesive indentation of soft, inhomogeneous materials (2007).
[33] D.C. Lin, E.K. Dimitriadis, F. Horkay, Robust strategies for automated AFM force curve analysis—II: adhesion-influenced indentation of soft, elastic materials (2007).
[34] A.R. Harris, G.T. Charras, Experimental validation of atomic force microscopy-based cell elasticity measurements, Nanotechnology 22 (2011) 345102.
[35] G.G. Bilodeau, Regular Pyramid Punch Problem, 1992.
[36] E. Makhija, et al., Mechanical strain alters cellular and nuclear dynamics at early stages of oligodendrocyte differentiation, Front. Cell. Neurosci. 12 (2018) 59.